Method for computing the three-dimensional capacity dimension from two-dimensional projections of fractal aggregates

F. Maggi[1,*] and J. C. Winterwerp[1,2,†]

[1]*Environmental Fluid Mechanics, Faculty of Civil Engineering and Geosciences, Delft University of Technology, P.O. Box 5048, 2600 GA, Delft, The Netherlands*

[2]*WL|Delft Hydraulics, P.O. Box 177, 2600 MH, Delft, The Netherlands*

(Received 20 August 2003; published 30 January 2004)

The current theory of projections of fractals is considered in this paper with application to fractal aggregates. In particular, this theory does not accurately enable the computation of the capacity dimension of three-dimensional aggregates from the capacity dimension of their two-dimensional projections. Herein we propose to compute the three-dimensional capacity dimension from the perimeter-based fractal dimension, using a semiempirical equation, an approach not applied earlier.

DOI: 10.1103/PhysRevE.69.011405 PACS number(s): 61.43.Hv

I. INTRODUCTION

Fractal geometry is widely recognized to be fundamental in scaling a variety of properties of aggregates of various nature. The fractal approach has been fruitfully employed, for instance, in sedimentology (mud flocs, bed structure [1–3]), chemistry (polymers, colloidal aggregates [4,5]), medicine (cancer growth, cell structure [6]), cosmology (galaxy distributions and patterns at large scales [7,8]), and many other disciplines dealing with fractal aggregates.

In general, analysis of fractal aggregates in $\mathbb{R}^3$ is based on optical projections in $\mathbb{R}^2$. However, the transformation of projection $\mathcal{P}:\mathbb{R}^3\rightarrow\mathbb{R}^2$ distorts the three-dimensional (3D) information of an aggregate, especially concerning its geometric organization. One of the most convenient tools to describe the geometric structure of a fractal set is the generalized dimensionality d_q, proposed by Hentschel and Procaccia in [9]. It is defined as follows: if we consider an ϵ covering $\subset\mathbb{R}^n$ by means of boxes of size ϵ of a fractal of length scale L, then $N=(L/\epsilon)^n=\ell^n$ is the total number of boxes in the domain. If N_i is the number of measuring points in the ith box and N_f the total number of points of the fractal, then $p_i=N_i/N_f$ determines the probability of a measuring point lying in the ith box. Consequently, the generalized dimensionality of the qth order is written as follows:

$$d_q=\frac{1}{1-q}\lim_{\epsilon\rightarrow 0}\frac{\ln\sum_{i=1}^{N}(p_i)^q}{\ln\epsilon}, \tag{1}$$

where q is a moment that gives strength to the probability p_i. The capacity dimension d_C [10], the information dimensions d_I [11–13] and the correlation dimension d_K [14] are special cases of d_q: $d_0=d_C$, $d_1=d_I$, and $d_2=d_K$, with $d_2\leqslant d_1\leqslant d_0\leqslant n$. A basic property of the generalized dimensionality is that $d_q=\text{const}\ \forall q$ for fully self-similar and homogeneous fractals (monofractal sets), while an infinite number of dimensions (all represented by d_q) is required to describe statistical self-similar, nonhomogeneous fractals (multifractal sets).

The dimensionality d_q has been further elaborated for application purposes into the corresponding multifractal spectrum $f(\alpha)$ and singularity strength $\alpha(q)$ [9,15–17]. These quantities describe any arbitrary mass-density distribution of a nonhomogeneous fractal [17,18] and its growth rate [14,19–22]. The relevance of evaluating the fractal properties of aggregates stems from those fundamental works. In substance, the possibility of determining the fractal dimensions of an aggregate from its projection would make the characterization of the aggregate more complete. In particular, the capacity dimension d_0 should be accessed as it plays a role in the nonlinear relationship between the mass M of an aggregate and its length scale L: $M\sim L^{d_0}$, and nevertheless in a number of other quantities such as the effective density, porosity, etc. [3,5,23].

However, direct computation of d_q from projections of real aggregates is limited by geometric constraints. This was shown by early investigations which were addressed to understand mathematically how projections $\mathcal{P}$ affect d_q [8,24]. In particular, Hunt and Kaloshin [24] have elaborated that $\mathcal{P}$ preserves the 3D information only for a limited range of moments q $(1<q\leqslant 2)$, thus leaving unsolved questions related to d_0, which have direct implication to applied sciences and measurement techniques.

The main contribution of this paper is to show that it is possible to extract the 3D capacity dimension of fractal aggregates from their projections by following an alternative path. The paper is organized as follows. Section II summarizes a literature-based survey on the theoretical limits to which d_q is subject in the case of projections of nonhomogeneous, *extensive* fractals. Furthermore, we give numerical evidence that the application of the theory to nonhomogeneous *finite* fractals yields distorted results, especially for the capacity dimension d_0. We infer that the finiteness of the sets causes these distortions (real fractal aggregates in contrast to extensive fractals). Section III is dedicated to the analysis of those results. In addition, we propose an analytical formulation capable of circumventing the limits exposed in Sec. II. This formulation is founded upon geometry arguments and fitting numerical results.

*Email address: f.maggi@ct.tudelft.nl

†Email address: han.winterwerp@wldelft.nl

II. PROJECTIONS AND GENERALIZED DIMENSIONALITY

A. Problem definition

Hunt and Kaloshin [24] have observed that the projection $\mathcal{P}:\mathbb{R}^m \rightarrow \mathbb{R}^n$ of a fractal $S_m \subset \mathbb{R}^m$ of generalized dimensionality $d_q(S_m)$ onto $\mathbb{R}^n$ (with $n<m$), yields to

$$d_q(S_n=\mathcal{P}(S_m))=\min\{n,d_q(S_m)\}. \tag{2}$$

If $d_q(S_m)>n$ then the projection S_n has dimensionality $d_q(S_n)=n$, otherwise $d_q(S_n)=d_q(S_m)$. When the projection has the same dimensionality as the original ($d_q(S_m)\leqslant n$), then $\mathcal{P}$ is called a *dimension-preserving* transformation. This relation has been proven analytically in [24] only for values of the moment $q:1<q\leqslant 2$. $\mathcal{P}$ is not dimension-preserving for $q\leqslant 1$ and $q>2$. In other words, only the correlation dimension d_2 and the infinite number of dimensions between d_2 and the information dimension d_1 are preserved. All other dimensions are not preserved, the capacity dimension d_0 included. This implies that for projections of real objects ($m=3$ and $n=2$), the capacity dimension $d_0(S_3)$ ($q=0$) cannot be found from Eq. (2):

$$d_0(S_2)\neq \min\{2,\, d_0(S_3)\}. \tag{3}$$

It follows that we cannot use the 2D capacity dimension $d_0(S_2)$ of a projection to characterize the 3D capacity dimension $d_0(S_3)$ of the original object in a direct way, at least theoretically, even when $d_0(S_3)<2$.

Moreover, Eq. (2) is deduced from the literature to be valid for indefinitely extensive fractals. However, no precise distinction has been made in literature for finite fractals, such as aggregates. For this reason, we must first consider whether Eq. (2) is applicable to 2D projections of fractal aggregates, because these are *nonhomogeneous*, *finite*, and *closed* (compact) sets. Indeed, images of fractal aggregates consist of the complete closed sets, that is the sets themselves and their boundaries. Furthermore, such sets are self-similar only over limited ranges of length scales. This is in contrast to self-similar (mono) fractal sets. Monofractals are, at least theoretically, open and homogeneous sets because any observation window replicates any other window, at any scale, according to the concept of self-similarity. The consequence of dealing with non-homogeneous finite and closed objects is that the application of Eq. (2) becomes less clear and liable to divergencies and misunderstandings [22].

We therefore compare in the next section theoretical values of $d_0(S_2)$ [via Eq. (2)] and numerical values (via computer simulations) of nonhomogeneous random fractals. From this test we will learn that Eq. (2) is not able to return accurate results, thus preventing the computation of $d_0(S_3)$ from $d_0(S_2)$. Next, we propose an alternative semi-empirical equation to compute $d_0(S_3)$ accurately.

B. Application of Eq. (2) to artificial fractal aggregates

Fractal aggregates are nonhomogeneous, finite, and closed random sets of connected seeds distributed within the domain. Furthermore, they are statistically self-similar with multifractal properties. Herein, we test the applicability of Eq. (2) on artificial aggregates.

We first generate n_r fractal aggregates $S_3 \subset \mathbb{R}^3$ by means of a simple algorithm which produces self-correlated random structures with known capacity dimension d_0. This technique is a *static* aggregation algorithm. Seed-by-seed diffusion or cluster-cluster reactions are not accounted for. Starting with a single (cubical) seed $i=1$, a second seed $i=2$ is placed randomly in one of the 3-by-3-by-3 free, neighbor locations. Then, one of the existing seeds is chosen from an exponential distribution, and a new seed is attached to it. In this algorithm, recent seeds (large indexes i) have higher probabilities to receive a new seed. This procedure is repeated for 1000 seeds. The capacity dimension $d_0(S_3)$ of the aggregate under construction is tuned by means of the exponent of the exponential distribution. The resulting sets S_3 are aggregates with few open branches, more similar to CCA aggregates than DLA aggregates [10,21]. The n_r sets S_3 are afterwards projected along the three Cartesian directions, thus obtaining the projections

$$\{S_{2,x}^{(j)}\},\{S_{2,y}^{(j)}\},\{S_{2,z}^{(j)}\}, \tag{4}$$

with $j=\{1,\ldots,n_r\}$ the repetition index. Three examples of $S_3^{(j)}$ and their projections are given in Fig. 1. For each of the $3n_r$ projections, we compute the capacity dimension d_0 according to Vicsek [10]:

$$d_0(S_{2,\{x,y,z\}}^{(j)},X)=\frac{\log[N]}{\log[X]}, \tag{5}$$

where N is the number of seeds in the projection and $X=\{L_2,L_3,D_2,D_3\}$ are the length scales taken into account. L is the size of the minimum hypercube enveloping S and D is the hydraulic diameter, in $\mathbb{R}^2$ and $\mathbb{R}^3$, respectively. The length scales $\{L_3,D_3\}\subset\mathbb{R}^3$ are known from the construction of the aggregates while the length scale $\{L_2,D_2\}\subset\mathbb{R}^2$ result from the transformation $\mathcal{P}$. Next, we compute the average capacity dimensions $\overline{d_0(S_2^{(j)})}$ of the projections for each j^{th} aggregate as follows:

$$\overline{d_0(S_2^{(j)},X)}=\frac{1}{3}[d_0(S_{2,x}^{(j)},X)+d_0(S_{2,y}^{(j)},X)+d_0(S_{2,z}^{(j)},X)]. \tag{6}$$

depending on the used length scales. The reason to consider different length scales comes from a misuse of them in the application to real cases.

Now, we consider the capacity dimension $d_0(S_3,\{L_3,D_3\})$, computed as a function of L_3 and D_3 solely.

The relationship between $\overline{d_0(S_2^{(j)},X)}$ and $d_0(S_3^{(j)},L_3)$ is given in Fig. 2, while the relationship between $\overline{d_0(S_2^{(j)},X)}$ and $d_0(S_3^{(j)},D_3)$ is given in Fig. 3. Both these experimental sets deviate largely from Eq. (2) for all the length scales here considered. In particular, Eq. (2) tends to overestimate the real values both for low- and high-dimensional aggregates.

Thus we have shown that, for nonhomogeneous, finite, and closed fractal aggregates, Eq. (2) does not enable a direct

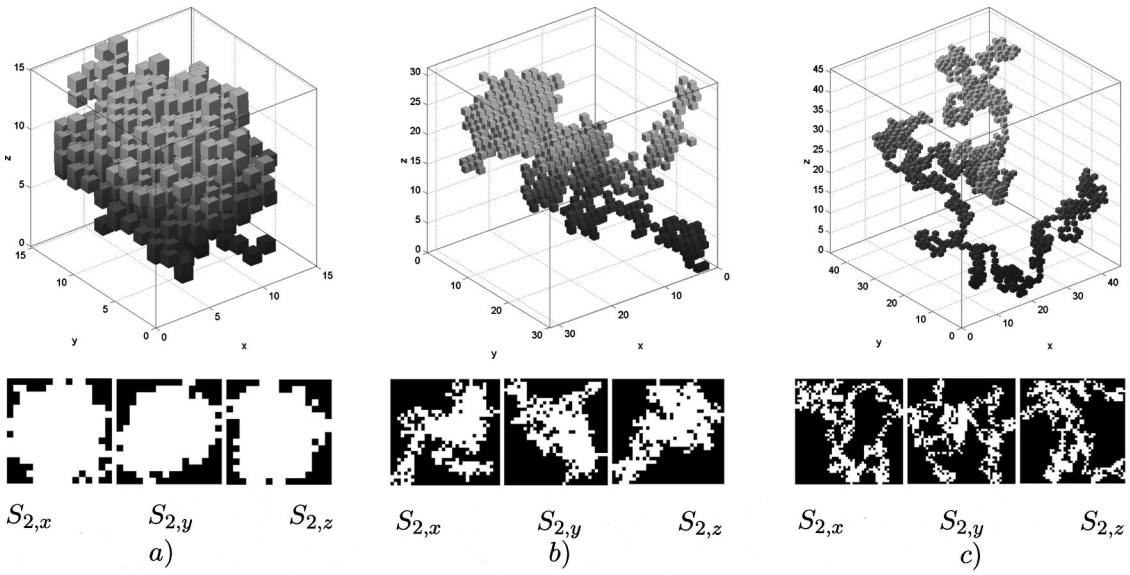

FIG. 1. (a) Example of a high-fractal-dimension aggregate, $S_3^{(1)}$, $d_0(S_3^{(1)})=2.49$. The projections show a massive and round-shaped organization of the primary particles. (b) Example of a mid-fractal-dimension aggregate, $S_3^{(14)}$, $d_0(S_3^{(14)})=2.09$. The projections show a less massive and irregular-shaped organisation of the primary particles. (c) Example of a low-fractal-dimension aggregate, $S_3^{(30)}$, $d_0(S_3^{(30)})=1.81$. The projections show a weak and irregular-shaped organization of the primary particles.

extraction of $d_0(S_3)$ from $d_0(S_2)$, even for $d_0(S_3)<2$. This was already stated in Eq. (2) and derived analytically in [24] for extensive fractals.

III. DIRECT COMPUTATION OF $d_0(S_3)$ FROM THE PROJECTION S_2

A. Perimeter of fractal sets

From the previous results, we have found confirmation that information concerning the *capacity* (the capacity dimension, that is the space-filling ability) is polluted by the projection itself, even for $d_0(S_3)<2$. Hence, we analyze another set belonging to the projection, which is independent or nearly independent of the transformation: the contour of the projected set S_2. The contour is a subset of the surface of S_3. The measure of the contour, that is the perimeter, does not represent a capacity of S_3. The perimeter, or better the perimeter segmentation reflects the roughness of the object in $\mathbb{R}^3$.

Herein, we investigate to which extent the information of the structure in $\mathbb{R}^3$ can be found in the projected, perimeter-based fractal dimension d_P, which is defined for instance in [21]. d_P does not belong (or give evidence of belonging) to the set of dimensions in d_q. As a consequence, the theory of

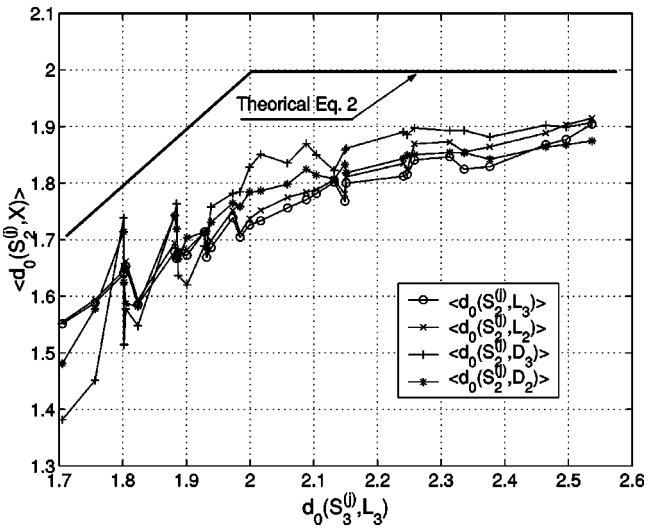

FIG. 2. 2D capacity dimension $d_0(S_2^{(j)},X)$ of the projections $S_2^{(j)}$ (dots) as a function of the 3D capacity dimension $d_0(S_3^{(j)},L_3)$. They have been compared to the theoretical relation, computed through Eq. (2) (solid line).

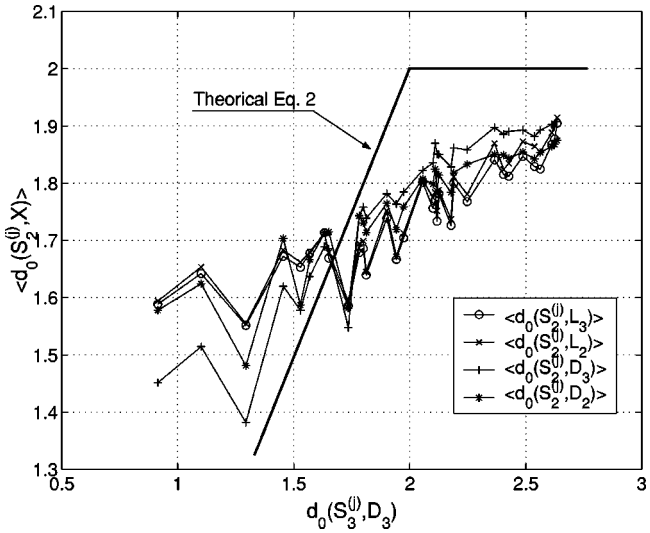

FIG. 3. 2D capacity dimension $d_0(S_2^{(j)},X)$ of the projections $S_2^{(j)}$ (dots) as a function of the 3D capacity dimension $d_0(S_3^{(j)},D_3)$. They have been compared to the theoretical relation, computed through Eq. (2) (solid line).

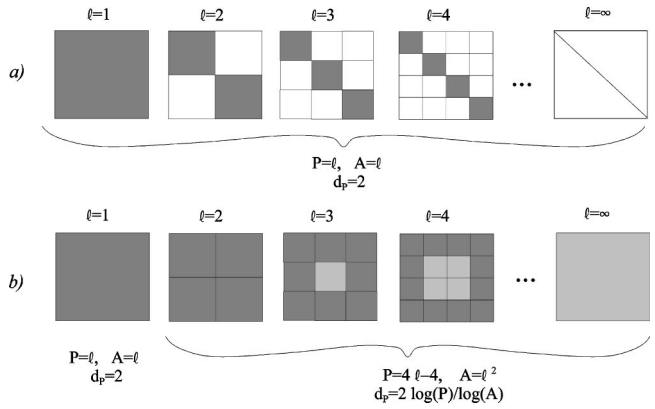

FIG. 4. Geometric representation of the limiting cases of (a) linelike projection and (b) fully massive projection as functions of the resolution ℓ. Dark gray boxes represent regions of perimeter/area overlapping, while light gray boxes belong solely to the area.

projection does not apply to d_P, and therefore it is not subject to the rule of Eq. (2). However, it still gives information on the fractal structures of aggregates. For this reason, and because of a lack of theoretical work dealing with this problem, we perform a simple numerical experiment on the correlation between $d_0(S_3^{(j)},L_3)$ and $d_P(S_2^{(j)})$, thus neglecting the length scales L_2, D_2, and D_3.

B. Perimeter-based fractal dimension of the projections

The perimeter-based fractal dimension d_P is defined according to [21]:

$$d_P=2\frac{\log[P]}{\log[A]}, \tag{7}$$

where P and A represent the perimeter and the area of a projection. Within our context, A is given by the number of seeds within the projected area and P is given by the number of seeds on the contour.

By means of simple geometry arguments, we compute the values of d_P for the two extreme cases of thin line and massive box projections. Let us therefore consider an ϵ covering of the set S_2 of length scale L_2 by means of boxes of size ϵ, corresponding to a resolution $\ell=L_2/\epsilon$. The values of d_P then depend on the resolution ℓ, as elaborated in the two following cases.

Thin line. Let us consider the case of a projection which becomes a thin line for increasing resolution $\ell\epsilon[1,\infty)$, Fig. 4(a). In that case

$$P\equiv A=\ell, \quad \ell\epsilon[1,\infty),$$

and, using Eq. (7), the resulting d_P becomes

$$d_P=2\frac{\log[P]}{\log[A]}=2\frac{\log[\ell]}{\log[\ell]}=2, \quad \ell\epsilon[1,\infty). \tag{8}$$

Massive box. Let us now consider a projection consisting of a massive box for resolutions $\ell\epsilon[1,\infty)$, Fig. 4(b). The generalized forms expressing the perimeter P and the area A are

$$P\equiv A=\ell, \quad \ell=1$$

$$P=4\ell-4, \ A=\ell^2, \quad \ell\epsilon[2,\infty),$$

from which we write Eq. (7) as a function of ℓ

$$d_P(\ell=1)=2\frac{\log[\ell]}{\log[\ell]}=2, \quad \ell=1$$

$$d_P(\ell=2)=2\frac{\log[4\ell-4]}{\log[\ell^2]}=2, \quad \ell=2 \tag{9}$$

$$d_P(\ell\geqslant 3)=2\frac{\log[4\ell-4]}{\log[\ell^2]}<2, \quad \ell\epsilon[3,\infty),$$

where the cases $\ell=1$ ($\epsilon=L$) and $\ell=2$ ($\epsilon=L/2$) represent two trivial solutions for d_P that can be referred to as a pathological effect caused by the low resolution. It is possible to see from Fig. 4(b) that $P\neq A$ for resolutions $\ell\geqslant 3$ ($\epsilon\leqslant L/3$). Hence, d_P decreases for increasing resolution. For $\ell\rightarrow\infty$ ($\epsilon\rightarrow 0$) we obtain the lower limit

$$\lim_{\ell\rightarrow\infty} d_P=\lim_{\ell\rightarrow\infty}\frac{\log[4\ell-4]}{\log[\ell]}=\lim_{\ell\rightarrow\infty}\left(\frac{\log[4]}{\log[\ell]}+\frac{\log[\ell-1]}{\log[\ell]}\right)=1, \tag{10}$$

which represents an asymptotic case for infinitely high resolutions of fully massive aggregates.

The limiting values of d_P are then represented by $d_P=2$ for linelike projections and $d_P=1$ for massive projections and infinitely high resolution.

C. Correlation analysis of $d_0(S_3)$ and $d_P(S_2)$

In order to investigate how $d_P(S_2)$ relates to $d_0(S_3)$, we first normalize the projections of Eq. (4) with a reference resolution ℓ_r. This is performed by using a magnification factor f_m defined as

$$f_m=\frac{\ell_r}{\ell}, \tag{11}$$

in such a way that

$$L_{2m}=f_m L_2=\ell_r\epsilon\forall S_2^{(j)}. \tag{12}$$

We compute the average perimeter-based fractal dimension $\overline{d_P(S_2^{(j)})}$ for the jth set $S_2^{(j)}$ as follows:

$$\overline{d_P(S_2^{(j)})}=\frac{1}{3}[d_P(S_{2,x}^{(j)})+d_P(S_{2,y}^{(j)})+d_P(S_{2,z}^{(j)})], \tag{13}$$

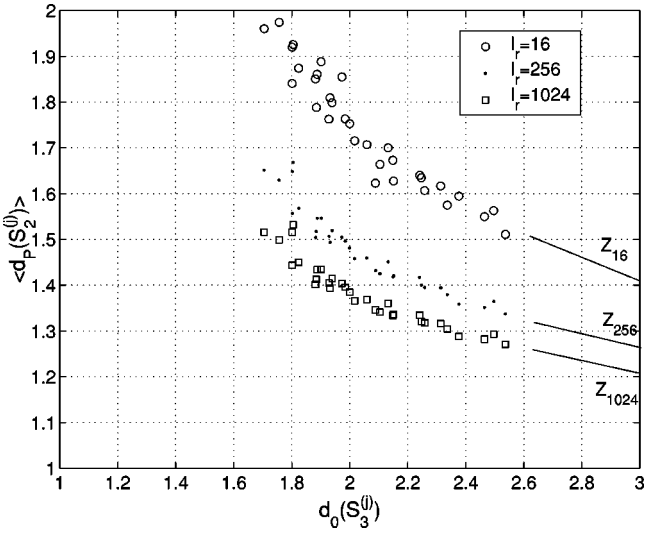

FIG. 5. Variation of $\overline{d_P(S_2^{(j)})}$ as a function of $d_0(S_3^{(j)},L_3)$ at different resolutions ℓ_r.

where d_P is defined in Eq. (7). In this computation we consider the external perimeter only, therefore neglecting inner empties.

Figure 5 shows the relationship between $d_P(S_2)$ and $d_0(S_3)$ for various resolutions, $\ell_r=\{16,256,1024\}$ pixels. Therein, we have evaluated the boundary points Z at $d_0(S_3)=3$ (massive box),

$$Z_{16}=(3,z(\ell_r=16)),$$

$$Z_{256}=(3,z(\ell_r=256)), \tag{14}$$

$$Z_{1024}=(3,z(\ell_r=1024)),$$

known by the analytical solution of Eq. (9), where we have applied the notation

$$z(\ell)=d_P(S_2,\ell)=\frac{\log[4\ell-4]}{\log[\ell]}. \tag{15}$$

There are three major features that we can observe from the results given in Fig. 5. The first is that low dimensional structures, with a high level of branching at the left-hand side of the plot, possess projections with high values of d_P. In contrast, high dimensional structures, with massive and round-shaped masses at the right-hand side of the plot, have low values of d_P. The second is that $d_P(S_2)$ does not reach a constant value for $d_0(S_3)>2$, in contrast to the rule of Eq. (2). Rather, a hyperboliclike correlation does appear in the full range $1\leqslant d_0(S_3)\leqslant 3$. The third is that low resolutions (16 pixels, for instance) move the points towards the upper limit $d_P=2$. An increase in resolution lowers the points asymptotically towards the limit $d_P=1$, as shown in Eq. (10).

These are valuable results that can be used to derive a semiempirical equation to relate $d_0(S_3)$ and $d_P(S_2)$ as a function of the resolution and with a hyperboliclike structure.

D. Semiempirical relation for $d_P(S_2)$ and $d_0(S_3)$

By considering the fully known points Z of Eq. (14) and assuming a function of the form

$$d_P(S_2)=\frac{a}{[d_0(S_3)]^2}+b, \tag{16}$$

we correlate the results in Fig. 5 by solving the following system in correspondence of the two points Z and K:

$$z(\ell)=\frac{a}{3^2}+b \quad \text{at } Z=(3,z(\ell)),$$

$$2=\frac{a}{[k(\ell)]^2}+b \quad \text{at } K=(k(\ell),2), \tag{17}$$

with $z(\ell)$ defined in Eq. (15). The coordinates $k(\ell)$ of the boundary points K at $d_P=2$ for a given resolution ℓ have been expressed as a function of $z(\ell)$ by fitting the data points in Fig. 5 at the upper limit $d_P=2$:

$$k(\ell)=k(z(\ell))=z(\ell)[z(\ell)-1]+1, \tag{18}$$

which results in

$$K_{16}=(k(\ell_r=16),2),$$

$$K_{256}=(k(\ell_r=256),2), \tag{19}$$

$$K_{1024}=(k(\ell_r=1024),2).$$

Hence, the coefficients a and b are

$$a(\ell)=9\left(z(\ell)-\frac{2[k(\ell)]^2-9z(\ell)}{[k(\ell)]^2-9}\right),$$

$$b(\ell)=\frac{2[k(\ell)]^2-9z(\ell)}{[k(\ell)]^2-9}. \tag{20}$$

Finally, Eq. (16) reads as a function of $d_0(S_3)$ and ℓ,

$$d_P(S_2)=\begin{cases}\dfrac{a(\ell)}{[d_0(S_3)]^2}+b(\ell) & \text{for } d_0(S_3)>k(z(\ell)),\\ 2 & \text{for } d_0(S_3)\leqslant k(z(\ell)).\end{cases} \tag{21}$$

Figure 6 shows the numerical results (dots) and the empirical fit (solid curves) obtained from Eq. (21) for resolutions $\ell_r=\{16,256,1024\}$ pixels. The fit for $\ell_r=16$ pixels is acceptable though not perfect ($R^2=0.970$). A better fit is obtained for resolutions $\ell_r=256$ pixels ($R^2=0.975$) and for $\ell=1024$ pixels ($R^2=0.973$), see Fig. 7. The correlation coefficients R^2 appear to have a maximum for a given resolution ($\ell_r=256$ in this case). Consequently, the reader can argue that the optimal determination of $d_0(S_3)$ occurs for a resolution $\ell<\infty$. However, we note that the fluctuation of the correlation coefficient is in the order of 10^{-3}; therefore,

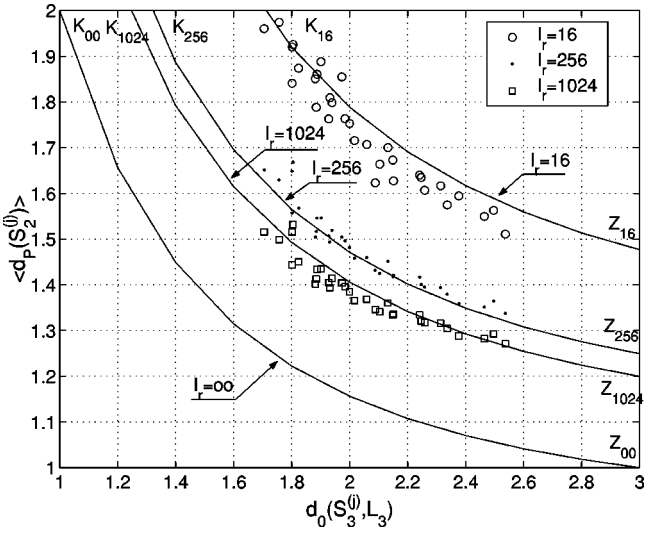

FIG. 6. Comparison of the numerical and analytical results from Eq. (21) at different resolutions ℓ_r.

statistically it is not relevant to infer any systematic trend or behavior. Besides this, the appreciable alignment of the data point supports the goodness of the technique proposed here.

By inversion of Eq. (21), we can write the following equation:

$$d_0(S_3)=\sqrt{\frac{a(\ell)}{d_P(S_2)-b(\ell)}} \quad \text{for } d_P(S_2)<2, \tag{22}$$

which gives the 3D capacity dimension of the aggregates from the perimeter-based fractal dimension of their projections and the adopted resolution.

E. The case of infinite resolution

For $\ell\to\infty$, the coordinates $z(\ell)$ and $k(\ell)$ of the boundary points Z and K of Fig. 6 become

$$z_\infty=\lim_{\ell\to\infty} z(\ell)=\lim_{\ell\to\infty}\frac{\log[4\ell-4]}{\log[\ell]}=1,$$

$$k_\infty=\lim_{\ell\to\infty} k(z(\ell))=\lim_{\ell\to\infty} z(\ell)[z(\ell)-1]+1=1. \tag{23}$$

and the coefficients of Eq. (20) are consequently

$$a=\frac{9}{8}, \quad b=\frac{7}{8}. \tag{24}$$

Equation (22) in the asymptotic limit $\ell\to\infty$ then becomes

$$d_0(S_3)=\sqrt{\frac{9/8}{d_P(S_2)-7/8}} \quad \text{for} \quad d_P(S_2)<2. \tag{25}$$

It matches the theoretical points $Z=(3,z_\infty)$ and $K=(k_\infty,2)$ as shown in Fig. 6.

F. Critical resolution

Equation (22) allows us to detect a critical resolution ℓ_c below which the computation of $d_0(S_3)$ is corrupted by low resolution. Let us consider a fractal aggregate with capacity dimension $d_0(S_3)=d^*$. If we want to be able to detect d^* by means of Eq. (22), then the condition

$$k(\ell)\leqslant d^*$$

must be satisfied. By expanding we obtain

$$[z(\ell)]^2-z(\ell)+1-d^*\leqslant 0.$$

Its corresponding solution is

$$z_1(d^*)\leqslant z(\ell)\leqslant z_2(d^*),$$

with

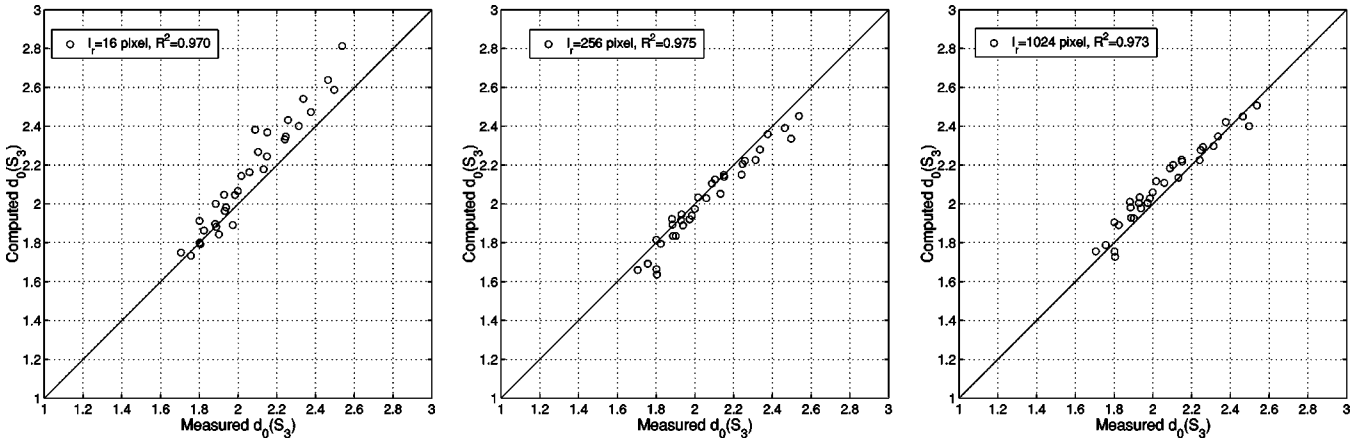

FIG. 7. Comparison of the parametrized values of $d_0(S_3)$ according to Eq. (22) versus the measured ones for the tested resolutions $\ell_r=\{16,256,1024\}$ pixels. Also the correlation coefficients R^2 are reported. The data points align along the bisector for exact, full correlation.

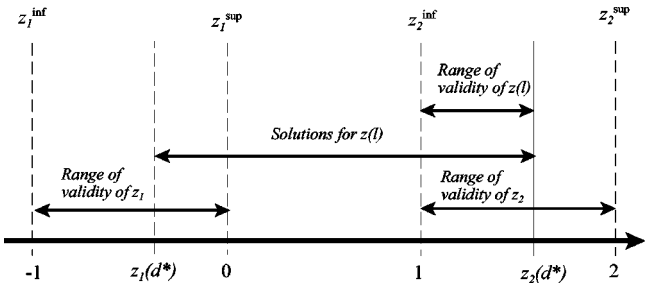

FIG. 8. Representation of the solution interval of the quantity $z(\ell)$. In particular, the range of validity of $z(\ell)$ is shown to be bounded in the range $[1,z_2(d^*)]$.

$$z_1(d^*)=\frac{1-\sqrt{-3+4d^*}}{2},$$

$$z_2(d^*)=\frac{1+\sqrt{-3+4d^*}}{2}. \tag{26}$$

If we consider that real aggregates possess capacity dimensions in the range $1\leqslant d^*\leqslant 3$, then the discriminant $\Delta=-3+4d^*$ is limited to the range $1\leqslant\Delta\leqslant 9$. In fact, if $S_3\subset\mathbb{R}^3$ then $d^*\leqslant 3$ for obvious physical limits. At the same time, if $d^*<1$ then the aggregate would consist of, at least, two disjointed, thin masses. This is not a unique aggregate anymore but two or more individual aggregates, with independent fates. Therefore, for the considered range of Δ, we obtain the ranges of validity of $z_1(d^*)$ and $z_2(d^*)$:

$$-1=z_1^{\inf}(d^*=3)\leqslant z_1(d^*)\leqslant z_1^{\sup}(d^*=1)=0,$$

$$1=z_2^{\inf}(d^*=1)\leqslant z_2(d^*)\leqslant z_2^{\sup}(d^*=3)=2.$$

The quantity $z(\ell)$ is $z(\ell)=d_P(S_2)$ as defined in Eq. (15); it is proven to lie in the range $[1,2]$ in Sec. III B. The resulting solutions of $z(\ell)$ are then limited to the positive range:

$$1\leqslant z(\ell)\leqslant z_2(d^*), \tag{27}$$

as represented in Fig. 8. In particular, since

$$z(\ell)\geqslant 1 \quad \forall\,\ell\,\epsilon[1,\infty),$$

we must satisfy only the condition

$$z(\ell)\leqslant z_2(d^*). \tag{28}$$

Therefore, in order to compute ℓ_c we substitute Eqs. (15) and (26) into Eq. (28),

$$z(\ell)=\frac{\log[4\ell-4]}{\log[\ell]}\leqslant\frac{1+\sqrt{-3+4d^*}}{2}=z_2(d^*),$$

$$\log[4\ell-4]\leqslant\frac{1+\sqrt{-3+4d^*}}{2}\log[\ell],$$

$$(4\ell-4)\leqslant\ell^{(1+\sqrt{-3+4d^*})/2}. \tag{29}$$

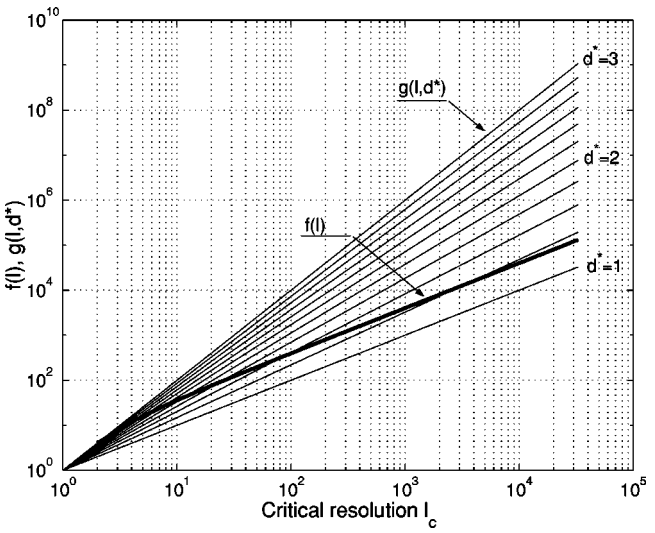

FIG. 9. Representation of the functions $f(\ell)$ and $g(\ell,d^*)$. The intersection points define the critical resolution ℓ_c below which the estimation of $d_0(S_3)$ through Eq. (21) is distorted by the low resolution.

Eventually, the transcendental function in ℓ of Eq. (29) can be rewritten for simplicity in the following form:

$$f(\ell)\leqslant g(\ell,d^*), \tag{30}$$

with $f(\ell)=(4\ell-4)$ and $g(\ell,d^*)=\ell^{(1+\sqrt{-3+4d^*})/2}$. In Fig. 9 we have represented the critical resolutions ℓ_c computed from the intersection of $f(\ell)$ and $g(\ell,d^*)$ through Eq. (30), for aggregates of various capacity dimensions d^* in $\mathbb{R}^3$. Figure 9 provides a practical tool for computing the minimum resolution required to be able to extract $d_0(S_3)$ from $d_P(S_2)$, once the observer can estimate the minimum expected $d_0(S_3)$.

IV. CONCLUSION

Current theory of the projection of fractals does not always enable direct computation of the capacity dimension of fractal sets embedded in $\mathbb{R}^3$ from the capacity dimension of projections in $\mathbb{R}^2$. This occurs in particular when the fractals under investigation are aggregates, that is finite and closed objects, with nonhomogeneous mass density distributions. In general, theoretical research tends to refer mostly to extensive fractals. However, in practice finite fractals are more likely to occur. Fractal aggregates differ considerably from indefinitely extended fractals. We have given evidence of the impact of the finite extent of fractals by means of comparisons of theoretical and numerical results in Figs. 2 and 3.

For these reasons, we have developed a method, circumventing the rule of Eq. (2) to obtain the 3D capacity dimension of aggregates from their projections. We neglect the information of ''capacity'' $d_0(S_2)$ present in the projections S_2, in favor of information concealed in the *perimeter* of the projection solely. To this end, a correlation analysis has been carried out to relate $d_0(S_3)$ to $d_P(S_2)$, using the perimeter-based fractal dimension d_P in $\mathbb{R}^2$. The results show that

$d_0(S_3)$ and $d_P(S_2)$ are related to each other by means of a hyperboliclike resolution-dependent function, defined in Eq. (21).

The expression here proposed to compute $d_0(S_3)$ from $d_P(S_2)$ allows us to derive analytically a critical resolution below which $d_0(S_3)$ cannot be calculated accurately. This has resulted in the nomogram of Fig. 9, which can be directly employed to estimate ℓ_c.

The accurate extraction of the capacity dimension of fractal aggregates obtained with Eq. (22) does not mean, however, that it can be successfully applied to any type of aggregated structure. The concept of *universality* is here involved for two reasons. The first is that Eq. (22) considers the information of perimeter segmentation, so that the internal area of the projections can be of any type: Euclidian or non-Euclidian. For Euclidian aggregates, only the external surface can be considered fractal, and not the complete object, thus there is no sense in computing a fractal dimension of a regular (Euclidian) structure. The second reason is that DLA and CCA processes produce different aggregate geometries [10,21]. At the moment we cannot state whether the perimeter segmentation is effectively capable of incorporating information on the geometrical structure in addition to the capacity of the structure. Therefore, future investigation must be oriented to understand whether Eq. (22) is valid for different aggregation kinematics (that is different structures), and not only for various capacity dimensions.

ACKNOWLEDGMENTS

The authors thank Professor Jurjen Battjes for his critical suggestions addressed during the development of the content exposed in this paper. This study was financed with Delft University Research funds through the BEO Program.

[1] J.C. Winterwerp, *On the Dynamics of High-concentration Mud Suspensions*, Ph.D. thesis (TUDelft Press, Delft, The Netherlands, 1999).
[2] J.C. Winterwerp, Cont. Shelf Res. **22**, 1339 (2002).
[3] C. Kranenburg, Estuarine Coastal Shelf Sci. **39**, 451 (1994).
[4] D.J. Jeffrey, Adv. Colloid Interface Sci. **17**, 213 (1982).
[5] K. Higashitani and K. Iimura, J. Colloid Interface Sci. **204**, 320 (1998).
[6] M. Keipes, F. Ries, and M. Dicato, Biomed. Pharmacother. **47(9)**, 409 (1993).
[7] P. Coleman and L. Pietronero, Phys. Rep. **213**, 311 (1992).
[8] R. Thieberger and E.A. Spiegel, Bull. Astron. Soc. India **30**, 461 (2002).
[9] H.G.E. Hentschel and I. Procaccia, Physica D **8**, 435 (1983).
[10] T. Vicsek, *Fractal Growth Phenomena* (World Scientific, Singapore, 1992).
[11] J. Balatoni and A. Rènyi, *Über den Begriff der Entropie, Arbeiten zur Informationstheorie I* (Deutscher Verlag der Wissenschaften, Berlin, 1957), pp. 117–134.
[12] C. Shannon, Bell Syst. Tech. J. **27**, 379 (1948).
[13] C. Shannon, Bell Syst. Tech. J. **27**, 623 (1948).
[14] H.G.E. Grassberger and I. Procaccia, Phys. Rev. Lett. **50**, 346 (1983).
[15] A. Chhabra and R.V. Jensen, Phys. Rev. Lett. **62**, 1327 (1989).
[16] M.H. Jensen, L.P. Kadanoff, and I. Procaccia, Phys. Rev. A **36**, 1409 (1987).
[17] T.C. Halsey, M.H. Jensen, L.P. Kadanoff, I. Procaccia, and B. Shraiman, Phys. Rev. A **33**, 1141 (1986).
[18] J. Argyris, G. Faust, and M. Haase, *An Exploration of Chaos*, edited by John Argyris, F.R.S. (North Holland, Amsterdam, 1994).
[19] T.C. Halsey, P. Meakin, and I. Procaccia, Phys. Rev. Lett. **56**, 854 (1986).
[20] C. Amitrano and A. Coniglio, Phys. Rev. Lett. **57**, 1016 (1986).
[21] P. Meakin, *Fractals, Scaling and Growth far from Equilibrium* (Cambridge University Press, Cambridge, England, 1998).
[22] L. Pietronero, Physica A **163**, 316 (1990); **163**, 324 (1990).
[23] F. Maggi, Delft University of Technology, Report No. 4-02, 2002.
[24] B.R. Hunt and V.Y. Kaloshin, Nonlinearity **10**, 1031 (1997).